Thermal probing in single microparticle and microfiber induced near-field laser focusing

Xiaoduan Tang,[1,2] Shen Xu,[1,2] and Xinwei Wang[1,*]

[1]*Department of Mechanical Engineering, Iowa State University, 2010 Black Engr. Bldg., Ames, IA, 50011, USA*
[2]*These authors contributed equally*
[*]*xwang3@iastate.edu*

Abstract: Microparticle and microfiber induced near-field laser heating has been widely used in surface nanostructuring. Information about the temperature and stress fields in the nanoscale near-field heating region is imperative for process control and optimization. Probing of this nanoscale temperature, stress, and optical fields remains a great challenge since the heating area is very small (~100 nm or less) and not immediately accessible for sensing. In this work, thermal probing of a single microparticle and microfiber induced near-field focusing on a substrate with laser light is conducted experimentally and interpreted by high-fidelity simulations. The laser ($\lambda = 532$ nm) serves as both heating and Raman probing sources. It is very interesting to note that variation of the Raman intensity, wavenumber, and linewidth all can be used to precisely capture the size of the micro-size subject on the substrate. Nanoscale mapping of conjugated optical, thermal, and stress effects, and the de-conjugation of these effects are performed. The effect of the laser fluence on the temperature and stress in the nanoscale heating region is investigated. With laser fluence of 3.9×10^9 W/m^2 and for a 1.21 μm silica particle induced laser heating, the maximum temperature rise and local stress are 58.5 K and 160 MPa, respectively. For a 6.24 μm glass fiber, they are 33.0 K and 120 MPa, respectively. Experimental results are explained and consistent with three-dimensional high-fidelity optical, thermal and stress field simulation.

OCIS codes: (350.4990) Particles; (160.2290) Fiber materials; (300.6450) Spectroscopy, Raman; (280.6780) Temperature; (310.4925) Other properties (stress, chemicals, etc.).

References and links

1. V. M. Shelekhina, O. A. Prokhorov, P. A. Vityaz, A. P. Stupak, S. V. Gaponenko, and N. V. Gaponenko, "Towards 3D photonic crystals," Synth. Met. **124**(1), 137–139 (2001).
2. G. Brambilla, F. Xu, P. Horak, Y. Jung, F. Koizumi, N. P. Sessions, E. Koukharenko, X. Feng, G. S. Murugan, J. S. Wilkinson, and D. J. Richardson, "Optical fiber nanowires and microwires: fabrication and applications," Adv. Opt. Photonics **1**(1), 107–161 (2009).
3. S. Jeong, L. Hu, H. R. Lee, E. Garnett, J. W. Choi, and Y. Cui, "Fast and scalable printing of large area monolayer nanoparticles for nanotexturing applications," Nano Lett. **10**(8), 2989–2994 (2010).
4. L. P. Li, Y. F. Lu, D. W. Doerr, D. R. Alexander, J. Shi, and J. C. Li, "Fabrication of hemispherical cavity arrays on silicon substrates using laser-assisted nanoimprinting of self-assembled particles," Nanotechnology **15**(3), 333–336 (2004).
5. E. McLeod and C. B. Arnold, "Subwavelength direct-write nanopatterning using optically trapped microspheres," Nat. Nanotechnol. **3**(7), 413–417 (2008).
6. M. Rycenga, P. H. C. Camargo, W. Y. Li, C. H. Moran, and Y. N. Xia, "Understanding the SERS effects of single silver nanoparticles and their dimers, one at a time," J Phys Chem Lett **1**(4), 696–703 (2010).
7. Y. Yue, X. Chen, and X. Wang, "Noncontact sub-10 nm temperature measurement in near-field laser heating," ACS Nano **5**(6), 4466–4475 (2011).
8. H. J. Münzer, M. Mosbacher, M. Bertsch, J. Zimmermann, P. Leiderer, and J. Boneberg, "Local field enhancement effects for nanostructuring of surfaces," J. Microsc. **202**(1), 129–135 (2001).

#184110 - $15.00 USD Received 24 Jan 2013; revised 9 Apr 2013; accepted 2 Jun 2013; published 7 Jun 2013

9. L. P. Li, Y. F. Lu, D. W. Doerr, and D. R. Alexander, "Laser-assisted nanopatterning of aluminium using particle-induced near-field optical enhancement and nanoimprinting," Nanotechnology **15**(11), 1655–1660 (2004).
10. S. M. Huang, M. H. Hong, B. S. Luk'yanchuk, Y. W. Zheng, W. D. Song, Y. F. Lu, and T. C. Chong, "Pulsed laser-assisted surface structuring with optical near-field enhanced effects," J. Appl. Phys. **92**(5), 2495–2500 (2002).
11. L. P. Li, Y. F. Lu, D. W. Doerr, D. R. Alexander, and X. Y. Chen, "Parametric investigation of laser nanoimprinting of hemispherical cavity arrays," J. Appl. Phys. **96**(9), 5144–5151 (2004).
12. X. Tang, Y. Yue, X. Chen, and X. Wang, "Sub-wavelength temperature probing in near-field laser heating by particles," Opt. Express **20**(13), 14152–14167 (2012).
13. X. Tang, S. Xu, and X. Wang, "Nanoscale probing of thermal, stress, and optical fields under near-field laser heating," PLoS ONE **8**(3), e58030 (2013).
14. V. Ng, Y. Lee, B. Chen, and A. Adeyeye, "Nanostructure array fabrication with temperature-controlled self-assembly techniques," Nanotechnology **13**(5), 554–558 (2002).
15. T. Hart, R. Aggarwal, and B. Lax, "Temperature dependence of Raman scattering in silicon," Phys. Rev. B **1**(2), 638–642 (1970).
16. S. Kouteva-Arguirova, T. Arguirov, D. Wolffframm, and J. Reif, "Influence of local heating on micro-Raman spectroscopy of silicon," J. Appl. Phys. **94**(8), 4946–4949 (2003).
17. T. Beechem, S. Graham, S. P. Kearney, L. M. Phinney, and J. R. Serrano, "Invited article: simultaneous mapping of temperature and stress in microdevices using micro-Raman spectroscopy," Rev. Sci. Instrum. **78**(6), 061301 (2007).
18. Y. W. Zheng, B. S. Luk'yanchuk, Y. F. Lu, W. D. Song, and Z. H. Mai, "Dry laser cleaning of particles from solid substrates: experiments and theory," J. Appl. Phys. **90**(5), 2135–2142 (2001).
19. M. R. Abel, "Thermal metrology of polysilicon MEMS using Raman spectroscopy," Master's Thesis (Georgia Institute of Technology, 2005).

1. Introduction

Micro/nanoparticles have outstanding optical properties and can be used to synthesize opaline colloidal crystals which exhibit photonic band gaps effect in the visible range [1]. Optical micro/nanofibers offer unique mechanical and optical properties, including large evanescent fields, high-nonlinearity, and strong optical confinement, which can be applied to reinforce plastics materials by improving their structural properties [2]. Nanotextured surfaces with enhanced physical and/or chemical properties can be produced using particles [3]. Large-area fabrication of nanoscale photonic structures using laser-assisted nanoimprinting of microparticles has been reported [4]. Arbitrary patterns and individual features at nanoscale have been achieved by employing a microsphere to focus a laser beam [5]. Surface-enhanced Raman scattering is mainly caused by the enhanced optical field on the surface of a metallic nanoparticle with localized surface plasmon resonance [6]. Another kind of near-field laser focusing is that induced by atomic force microscopy (AFM) tips. Nanoscale temperature probing of silicon under AFM tip focused laser heating has been conducted using Raman thermometry [7].

In laser-assisted nanolithography using microparticles, very high temperature rise and stress can be induced. Knowledge of the thermal and stress information in the near-field heating region under particles is critical for process control and optimization. Theoretical simulations about particle-induced near-field focusing have been reported in the past. Calculations of the intensity enhancement near a dielectric particle under laser illumination were performed based on the Mie scattering theory [8]. Electric field distributions within a particle above a substrate under laser irradiation were obtained [5, 9, 10]. Moreover, the temperature of a substrate beneath particles with laser irradiation was calculated [10, 11]. The thermal response inside the substrate under laser-irradiated particle is very difficult to probe experimentally as the near-field focusing area is immediately below the particle at the nanoscale. In our previous work, the temperature information inside silicon under self-assembled particles induced laser heating has been retrieved [12]. Far-field nanoscale imaging of conjugated thermal, mechanical (stress) and structural effects was also conducted on two-dimensional array of particles [13]. However, the measured temperature rise and stress is a collective effect by many particles. No effort has been reported on the Raman scattering and thermal probing in single particle and single fiber induced near-field focusing. It is always of

#184110 - $15.00 USD Received 24 Jan 2013; revised 9 Apr 2013; accepted 2 Jun 2013; published 7 Jun 2013

great interest to study the laser focusing behavior in a substrate under a single particle and a single fiber.

In this work, far-field nanoscale mapping of conjugated structural, thermal, and stress effects in silicon beneath a single microparticle and microfiber is conducted for the first time using Raman spectroscopy. The structural, thermal, and stress effects are de-conjugated from the Raman mapping. The thermal response of a silicon substrate beneath single silica particle and glass fiber with laser irradiation is performed. The intensity, temperature, and stress fields inside silicon are modeled to interpret the measurement results. Our experimental work on nanoscale thermal and stress probing has great potential applications in nanolithography and nanotexturing in terms of process control and surface structure tailoring.

2. Experimental details

Figure 1(a) shows schematic of the experimental setup for the near-field focusing. The Raman scattering system consists of a confocal Raman spectrometer (Voyage^{TM}, B&W Tek) and a microscope (Olympus BX51). The laser beam ($\lambda = 532$ nm) is focused by a $100\times$ objective lens (NA=0.80), and uniformly distributed in space. The movements of the sample are controlled by a piezo-actuated nano-stage (ThorLabs NFL5DP20) in the *x* direction and a motorized micro-stage (ThorLabs MT1-Z8) in the *z* direction. The piezo-actuated range of the nano-stage is 20 μm with a resolution of 20 nm. The control range of the micro-stage is 12 mm with a resolution of 0.1 μm . With a locking screw, the micro-stage can remain at a desired vertical position without drift during the experiment. The incident laser used as both Raman probing and heating source is focused on a single silica particle by the objective lens. Due to the focusing effect of the particle, the laser beam is further focused on the silicon substrate and heats it up. The sample consists of several single 1.21 μm silica particles (Bangs Laboratories) and a silicon (100) substrate (University Wafer). Single particles are patterned on a wafer using a tilting technique [14]. Monodisperse particle suspensions mixed with surfactant (triton-X : methanol = 1:400 by volume) are dispensed onto a wafer using a syringe and left to dry for 0.5 h in the air. The wafer is tilted on a table with an angle of about $10°$ to help with the flow of the mixture solution on the wafer. Single isolated silica particles on the silicon wafer can be identified under an optical microscope and are used for near-field optical effect probing. Figure 1(b) shows scanning electron microscope (SEM, FEI Quanta 250) images of single silica particles on a silicon wafer. The diameter of the particles is about 1.20 μm , while the laser spot size is about 0.5 μm under $100\times$ magnification. The laser spot size is determined using a blade method. By moving a blade along two perpendicular directions to shade the laser beam, the laser energy is found decreasing linearly with the moving distance. The laser spot length covering 90% of the laser energy is chosen to represent the spot size.

To conduct the Raman mapping experiments, a microparticle is identified under the microscope. The Raman intensity reaches its maximum value where the laser beam is focused on the particle center. A 3-D scanning process is employed to determine this focusing position. During this process, the sample is scanned along the *y* direction covering the particle center with a step of 53 nm. Raman spectra are obtained at all these positions and compared to determine the location where the maximum Raman intensity appears. Then the sample is moved back to the position where the maximum Raman intensity in the *y* direction is located. There is no sample movement in the *y* direction in the following process. A similar process is taken to determine the focusing position in the *x* direction. The scanning process in the *z* direction is followed in order to determine the focal level. Raman spectrum is affected by the focal level even other environmental factors are fixed. Raman intensity and wavenumber decrease, and linewidth (FWHM: full width at half maximum) broadens when the sample moves away from the focal plane in the *z* direction [12]. Raman intensity would decrease by at least 5% when the sample position is of 533 nm distance from the laser focal position. In

#184110 - $15.00 USD Received 24 Jan 2013; revised 9 Apr 2013; accepted 2 Jun 2013; published 7 Jun 2013

the experiments, the position of the sample is adjusted near the focal plane and Raman spectra are obtained at each focal level. The focal level is selected with the highest Raman intensity in the z direction. Now the sample is located where maximum intensity exists in all the three dimensions. The position of the sample in the y and z directions is then fixed. The sample is moved away from the center of the particle in the x direction to start the mapping experiment. The sample is scanned along the x direction as shown in Fig. 1(c). The movement is controlled electrically without any touch of the sample, stage, Raman spectrometer, microscope and other related equipment that would affect the quality of Raman signal. The variation of Raman spectra with the sample location is achieved at the nanoscale.

To evaluate the temperature rise and thermal stress in the particle-induced near-field laser focusing, experiments on silicon with single particles on its surface and bare silicon with no particles are both performed. A 3-D scanning process as mentioned above is also carried out to determine the focusing position. The incident laser is focused on one single particle on the Si substrate, and the Raman spectra are taken under four energy levels. Bare silicon is located around the particle. Raman spectra of bare silicon are obtained under four energy levels after shifting the particle away to allow direct laser irradiation on bare silicon. The integration time and measurement average are all the same (detailed later). A group of data for Raman spectra at different focal levels around the focal plane is obtained for each case. The Raman spectrum with the highest intensity is selected to represent each result. The environmental differences among those cases are extremely minimized, and the temperature rise and local stress are determined.

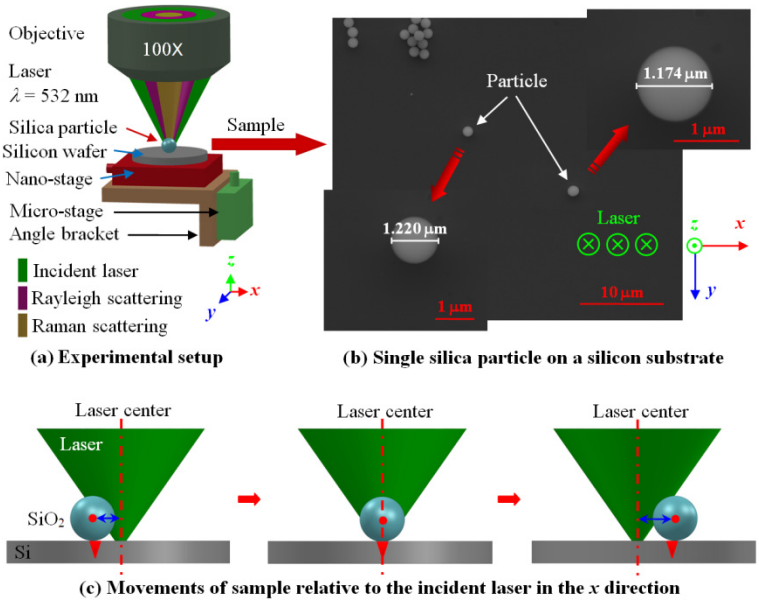

Fig. 1. Schematic of experimental setup for near-field thermal probing (not to scale). (a) A sample is located under an objective-focused laser beam from a Raman spectrometer. The movement of sample in the x direction is controlled by a piezo-actuated nano-stage. The focal level of the laser on the sample in the z direction is controlled by a motorized micro-stage. (b) The sample consists of a silicon substrate and a monolayer of silica particles. The spot size of the incident laser is about 0.5 μm in the x-y plane on a silicon substrate. (c) During the experiment, the position of the laser beam is fixed, and the sample moves along the x direction controlled by the nano-stage electrically without any touch of the sample and other equipment.

#184110 - $15.00 USD Received 24 Jan 2013; revised 9 Apr 2013; accepted 2 Jun 2013; published 7 Jun 2013

3. Results and discussion

3.1 Near-field focusing under a single microparticle

A single silica particle is identified under the confocal microscope for imaging. Raman excitation laser is focused on the single particle. Raman mapping for silicon beneath the single particle is obtained under laser irradiation of 3.7×10^9 W/m^2 with an integration time of 2 s. Each Raman spectrum is measured 3 times automatically and averaged. The Gaussian function is employed to fit the experimental Raman data. The particle is moved relative to the laser along the x direction within a range of 3 μm with a step of 53 nm. The Raman intensity I of silicon first increases and then decreases with the movement of sample [Fig. 2(a)]. The difference between the highest (I_{max}) and lowest (I_{min}) Raman intensities is 8000, with an intensity ratio (I_{max}/I_{min}) of 3.86. The distance from I_{max} decreasing to I_{min} is 692 nm. Within a distance of 20 nm in the x direction, the intensity difference and intensity ratio are 400 and 1.08, respectively. As the intensity is the raw datum without any further processing, and it can reflect the surface change of the sample, so it is the best quality to evaluate the imaging resolution. It is conclusive that the imaging resolution based on the Raman intensity difference can be down to 20 nm, although the step length in the experiments is 53 nm. During the imaging process, wavenumber ω first increases from 519.1 to 520.0 cm^{-1}, and then keeps constant. At position I in Fig. 2(a), as part of the particle is under laser irradiation, ω starts to increase. At position II, I reaches its maximum I_{max}, where ω is about 520.2 cm^{-1}. ω continues increasing to its maximum (520.5 cm^{-1}) at position III within a distance of 319 nm, and then decreases to its minimum. Linewidth Γ changes in a range from 6.3 to 8.0 cm^{-1}, with a maximum difference of 1.7 cm^{-1}. The variation tendency of Γ is contrary to that of ω. It first decreases and then increases.

The increasing and decreasing distances for I and ω are not equal, and the positions of their maximums are not coincident. Figure 2(b) illustrates the mechanism behind these phenomena. The beam axis of the excitation laser (black line) and the signal collecting axis of the Raman spectrometer (red line) are off a little (not exactly confocal). The two axes are not exactly parallel (confocal). The Raman spectrometer, excitation laser, and microscope are designed to be confocal. However, due to the accuracy of the assembling process and the vibration during the transportation of the equipment, misalignment at a scale of a few hundreds of nanometers occurs and it is difficult to avoid. For a regular sample with flat surface, the effect of the misalignment is not significant. However, the sample used in our experiment is a substrate with a focusing element (microparticle) on the surface. In addition, the diameter of the particle is comparable with the scale of the misalignment. Thus, the misalignment becomes an important factor in obtaining high measurement accuracy. In our experiments, when the sample moves relative to the laser beam, the varying angle of the scattered signal coming into the spectrometer leads to a virtual spectral change in the detector, and the variations of Raman curves are not symmetric. The relative positions of the particle to the laser beam axis and Raman signal collecting axis are corresponding to the same marks in Fig. 2(a). At position I, the laser irradiates the right part of the particle and is focused on the substrate. As the laser beam axis is of distance from the signal collecting axis, the Raman scattering signals, which come back to the objective, are not at the focal plane. This out-of-focus effect leads to the variation of Raman signals. It would decrease I and ω. At position II, the laser focal spot through the particle is coincident with the laser beam axis. Raman scattering signals are most excited and I_{max} exists. The laser focal point is near the Raman signal collecting axis but not coincident. As a result, the out-of-focus effect still exists. ω keeps increasing and I continues decreasing when the particle moves towards position III. At position III, the laser focal spot is at the signal collecting axis of the Raman spectrometer. Raman scattering signals are accurately collected by the spectrometer. There is no out-of-focus effect at position III. ω reaches its maximum because the collected Raman signals are

#184110 - $15.00 USD Received 24 Jan 2013; revised 9 Apr 2013; accepted 2 Jun 2013; published 7 Jun 2013

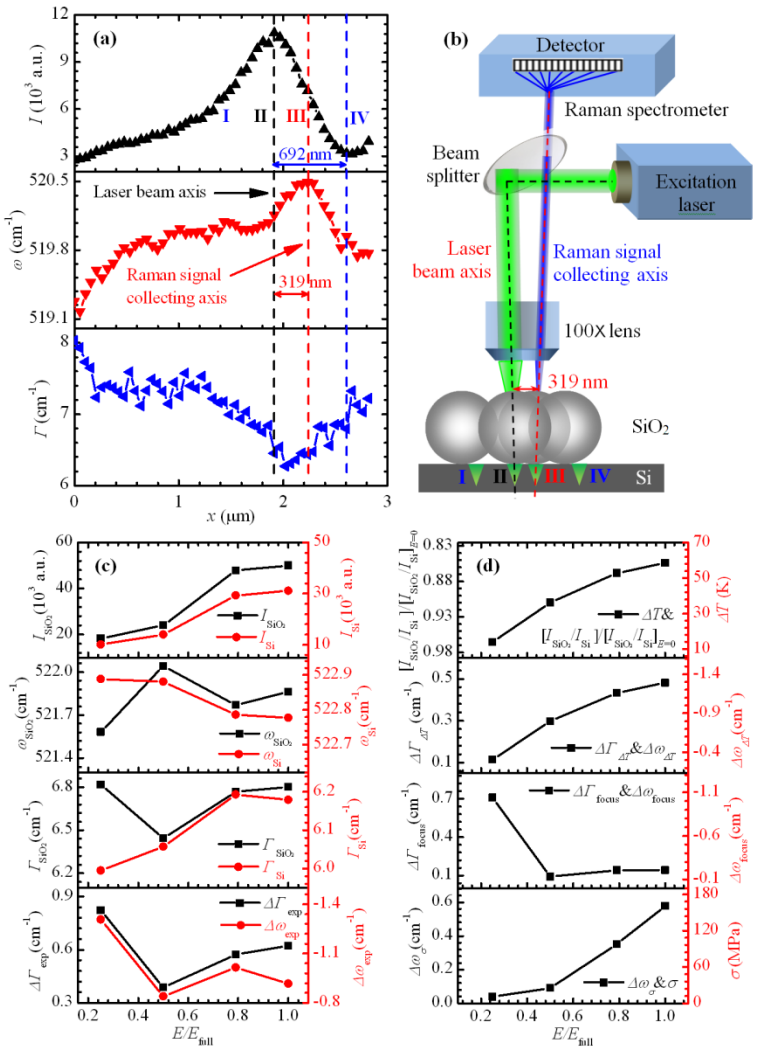

Fig. 2. Raman mapping and thermal probing inside silicon under single-particle-focused laser irradiation. (a) The x direction variation of Raman intensity I, wavenumber ω, and linewidth Γ for silicon under particles of 1210 nm diameter with laser irradiation. (b) The position of a silica particle relative to the laser beam axis and Raman signal collecting axis to explain the observed Raman variation in space. (c) How Raman data of silicon under 1210 nm silica particle and that of pure silicon vary with energy percentage. (d) Temperature rise and thermal stress in silicon under different laser energies.

from the focal plane of the Raman collecting optical path. I is not quite high as part of the particle is outside of the laser beam. From position III to IV, the collected Raman signal becomes more out of focus, so I and ω go down. In addition, I becomes weaker as the particle moves out of the laser beam. Based on this analysis and the distance between I_{max} and ω_{max}, we conclude that the laser beam axis and the Raman signal collecting optical path is off by about 319 nm under the 1210 nm particle near-field focusing. For different focusing elements, such as a microfiber, with different diameters, the focusing conditions are different due to the geometry difference. The offset of the two axes on the sample would be different, which will be demonstrated in the next section.

For the nanoscale imaging based on Raman intensity, wavenumber, and linewidth, their variation against location reflects combined effects of near-field optical heating, local stress,

#184110 - $15.00 USD Received 24 Jan 2013; revised 9 Apr 2013; accepted 2 Jun 2013; published 7 Jun 2013

and structural variation in space. These three effects are de-conjugated in this section to obtain quantitative information about the nanoscale local stress and temperature. To do this, the Raman spectra for silicon under a silica particle and those for bare silicon are compared. Four laser energy levels of 25%, 50%, 79%, and 100% are used in our experiments, with a full energy flux (E_{full}) of 3.9×10^9 W/m^2. The temperature rise is first evaluated based on the Raman intensity ratio. The Raman spectra at various focal levels and sample positions are obtained. Position II, as shown in Fig. 2(a), is selected to determine the thermal response in silicon. At position II, the laser focal spot under the particle is coincident with the laser beam axis. The excited Raman signals reach maximum. The Raman intensity at this position is the highest. When the position of the particle and other factors are fixed, the Raman intensity is mainly affected by two factors. One is the focal level in the vertical direction, and the other is the temperature rise. The intensity will change a lot even if there is only a small change in focal level. Compared with the intensity change caused by focal level, the intensity decrease induced by temperature rise is small. To make sure the focal level is selected the same for the cases at different energies, the Raman signals with maximum Raman intensities are chosen to represent the results. The Raman intensity for silicon under a silica particle (I_{SiO_2}) is higher than that for bare silicon (I_{Si}) due to near-field focusing, as shown in the first panel of Fig. 2(c). Raman intensity can be expressed as $I = f_1 f_2 f_3(\Delta T) f_4$, where f_1 denotes the effect of the system optical alignment; f_2 represents the laser energy effect, which indicates that the Raman intensity change is proportional to the laser energy; $f_3(\Delta T)$ is the intensity variation induced by the temperature rise; and f_4 the focusing element effect (here the element is a microparticle) including laser focusing and scattering influence. For silicon with a silica particle on its top, we have $I_{\text{SiO}_2} = f_1 f_2 f_3(\Delta T) f_4$. But for bare silicon, we have $I_{\text{Si}} = f_1 f_2$. Here $f_3(\Delta T) = 1$ as the temperature rise is negligible due to the large thermal conductivity of silicon. $f_4 = 1$ as there is no particle on the substrate. I_{Si} is acquired immediately after I_{SiO_2} , so f_1 and f_2 are the same for both I_{Si} and I_{SiO_2} . Thus, the intensity ratio is only relative to the temperature rise and particle-induced laser focusing condition as $I_{\text{SiO}_2}/I_{\text{Si}} = f_3(\Delta T) f_4$. The Raman intensity of silicon decreases with the increase of temperature for the reason that high temperature changes the band structure in silicon, and it restricts the photon interactions necessary to generate Raman signals. The temperature dependence of Raman intensity has been calibrated in our previous work [12]. The normalized Raman intensity of silicon decreases with temperature at a slope of -0.00249 K^{-1} within a temperature range of 290 - 440 K. In this experiment, the normalized intensity ratios at different energy levels are determined to evaluate the temperature rise. First of all, we obtain the original intensity ratio: $I_{\text{SiO}_2}/I_{\text{Si}}$, then based on this ratio change against the last energy, extrapolation is conducted to determine the ratio at zero laser energy $\left[I_{\text{SiO}_2}/I_{\text{Si}}\right]_{E=0}$. To eliminate the effect of particle-induced laser focusing condition (f_4), the normalized intensity ratio is introduced as $\left[I_{\text{SiO}_2}/I_{\text{Si}}\right] \Big/ \left[I_{\text{SiO}_2}/I_{\text{Si}}\right]_{E=0}$. The normalized intensity ratio is only dependent on the temperature rise, and is shown in the first panel of Fig. 3(d). The percentage of intensity decrease determines the amount of temperature rise in silicon. According to the calibrated slope, the temperature rise (ΔT) increases from 13.8 to 58.5 K when the energy level goes up from 25% to 100%. The uncertainty of temperature rise can evaluated according to the uncertainty of intensity ratio at zero laser energy, which is 0.01167. Based on the relationship between intensity ratio and temperature change (-0.00249 K^{-1}), the error level of temperature rise is ± 4.7 K.

#184110 - $15.00 USD Received 24 Jan 2013; revised 9 Apr 2013; accepted 2 Jun 2013; published 7 Jun 2013

In order to determine the thermal stress σ inside silicon, combined use of wavenumber ω and linewidth Γ is necessary. When the temperature of the material increases, ω decreases and Γ broadens [15]. Γ is stress insensitive to the first order, while stress causes a shift in ω [16, 17]. Considering the temperature rise and out-of-focus effect for silicon, the experimental linewidth broadening can be expressed as $\Delta\Gamma_{\text{exp}} = \Delta\Gamma_{\Delta T} + \Delta\Gamma_{\text{focus}}$, where $\Delta\Gamma_{\Delta T}$ is due to temperature rise; and $\Delta\Gamma_{\text{focus}}$ is because of the out-of-focus effect. For Raman wavenumber softening, $\Delta\omega_{\text{exp}} = \Delta\omega_{\Delta T} + \Delta\omega_{\text{focus}} + \Delta\omega_{\sigma}$, where $\Delta\omega_{\Delta T}$ is due to temperature rise; $\Delta\omega_{\text{focus}}$ is because of the out-of-focus effect; and $\Delta\omega_{\sigma}$ is induced by thermal stress. Raman linewidth of silicon increases linearly with temperature and the slope is 0.0082 cm^{-1}/K, and the slope for the wavenumber softening against temperature is –0.022 cm^{-1}/K [12]. Based on the temperature rise (ΔT) calculated from the intensity ratio, $\Delta\Gamma_{\Delta T}$ and $\Delta\omega_{\Delta T}$ can be obtained according to the slope, and the results are shown in the second panel of Fig. 2(d). So $\Delta\Gamma_{\text{focus}} = \Delta\Gamma_{\text{exp}} - \Delta\Gamma_{\Delta T}$, and the result is shown in the third panel of Fig. 2(d). $\Delta\omega_{\text{focus}}$ needs to be calculated from $\Delta\Gamma_{\text{focus}}$. The experiments to determine the relation between wavenumber and linewidth at different focal levels have been conducted in our lab [12]. The experimental data give a relation of $\Delta\omega_{\text{focus}} = -0.21055 - 0.76742\Delta\Gamma_{\text{focus}}$, and the result is also included in the third panel of Fig. 2(d). The wavenumber shift induced by stress is given by $\Delta\omega_{\sigma} = \Delta\omega_{\text{exp}} - \Delta\omega_{\Delta T} - \Delta\omega_{\text{focus}}$, and the values are shown in the fourth panel of Fig. 2(d). A relation between the shift of wavenumber $\Delta\omega_{\sigma}$ and the stress σ inside silicon has been developed with a proportionality constant of –3.6 cm^{-1}/GPa [17]. This calibration is for bulk silicon. In our work, the thermal stress existing region is at nanoscale (~100 nm). Such size difference will not affect the validity of the calibration result. This is because in our work, the Raman signal collecting region is large enough for statistical average and to reflect the structure change (stress). Finally, the thermal stress σ inside silicon is acquired according to the relation, and is shown in the fourth panel of Fig. 2(d). In Fig. 2(d), σ increases from 10 to 160 MPa as energy level goes up from 25% to 100%. The uncertainty of σ can be calculated from that of $\Delta\omega_{\sigma}$, which is $\Delta\omega_{\sigma} = \Delta\omega_{\text{exp}} - \Delta\omega_{\Delta T} - \Delta\omega_{\text{focus}}$. The experimental error of ΔT is $\pm$ 4.7 K. Based on the relationship between wavenumber and temperature (–0.022 cm^{-1}/K), the uncertainty of $\Delta\omega_{\Delta T}$ is $\pm$ 0.10 cm^{-1}. The experimental error of $\Delta\omega_{\text{exp}}$ is $\pm$ 0.02 cm^{-1}. Here the error of $\Delta\omega_{\text{focus}}$ is pretty small, which can be negligible. Thus, the combined standard uncertainty of $\Delta\omega_{\sigma}$ is determined as about $\pm$ 0.10 cm^{-1}. σ is proportional to $\Delta\omega_{\sigma}$ with a slope of –3.6 cm^{-1}/GPa, so the uncertainty of thermal stress is $\pm$ 28 MPa. The thermal stress goes up as local temperature increases for the reason that the thermal stress is induced by the temperature gradient in space. The particle-focused laser beam heats up the silicon under the particle within a very small area around 200 nm in radius (detailed in the modeling section). The localized heating by the laser beam causes thermal expansion in the heated area which is constrained by the nearby cold silicon. This constraint places a compressive stress in the heated region. The stress in silicon caused by the weight of particle is negligible. Assume the diameter of the contacting area between particle and substrate is 10 nm, then the pressure ($p = \rho V g/A$) on the substrate is only about 0.3 kPa, where ρ is the density of silica, V is the particle volume, g is acceleration of gravity, and A is the contacting area.

3.2 Near-field focusing by a single silica microfiber

To explore the near-field effect in silicon beneath a single microfiber under laser focusing, the mapping and thermal probing experiments are conducted with a 6 μm glass fiber. Figure 3(a) shows SEM images of a glass fiber (Mo-Sci Corp.) on a silicon wafer. The average diameter

#184110 - $15.00 USD Received 24 Jan 2013; revised 9 Apr 2013; accepted 2 Jun 2013; published 7 Jun 2013

of the glass fiber is 6.24 μm . A 3-D scanning process is employed to ensure the laser focusing position. Raman mapping experiments are carried out twice for silicon beneath a single glass fiber under laser irradiation of 3.1×10^9 W/m^2. The laser is focused on the silicon after passing the glass fiber. The sample moves relative to the laser along the *x* direction in a range of 16 μm with a step of 267 nm. The integration time is 4 s. Figure 3(b) illustrates the variations of I, ω, and Γ with *x* for the first imaging experiment. As little difference is found between the two imaging experiments, only the first one is analyzed in detail. When the laser beam approaches the glass fiber, I first decreases to $I_{\min}$, and ω increases to $\omega_{\max}$. This is because only a small portion of the laser beam is focused by the glass fiber at a position of about 2-3 μm away from the objective center in the *x* direction, and the Raman signal is mostly missed by the collecting system. At position I as shown in Fig. 3(b), the fiber center moves closer to the laser beam axis; both I and ω start to increase after passing position I. When the laser beam axis and the fiber center are coincident (position II, black line), I reaches $I_{\max}$, but ω would continue rising a little bit due to the out-of-focus effect. At position III, the laser focal center meets the signal collecting axis of Raman spectrometer (red line). I is a little smaller than $I_{\max}$ and ω reaches $\omega_{\max}$. There is no out-of-focus effect at this situation. Then the fiber moves away from the laser beam, and the variations of I and $\omega_{\max}$ are reverse to the situation of that the fiber approaches the laser beam. The maximum intensity difference ($I_{\max}$ - $I_{\min}$) is 10600, with an intensity ratio ($I_{\max}/I_{\min}$) of 3.56. The distance between the two $I_{\min}$ is 6.132 μm , close to the fiber diameter (6.240 μm). ω changes in a range from 518.6 to 520.8 cm^{-1}, and Γ varies from 8.1 to 10.6 cm^{-1}. The variation of Γ is contrary to that of ω. As shown in Fig. 3(b), we see more complicated variation of ω and Γ against the location than that for the single particle discussed in the last section. This is largely due to the geometry complication induced by the large size of the fiber.

Raman spectra for silicon under glass fiber and those for bare silicon are compared [Fig. 3(c)] to de-conjugate the combined effect of near-field optical heating, temperature, and stress variation in space. Four laser energy percentages of 25%, 50%, 79%, and 100% are used with the highest energy flux of 3.9×10^9 W/m^2. Raman spectra for both cases are taken at different focal levels near the focal spot to find the highest Raman intensities. The Raman spectra at position II as shown in Fig. 3(b) are chosen for analysis, where intensity reaches its maximum. Figure 3(c) shows the Raman intensity for silicon under glass fiber (I_{GF}) and that for bare silicon (I_{Si}). Also shown in Fig. 3(c) are the related wavenumber and linewidth. The integration time for I_{GF} and I_{Si} is 8s and 4s, respectively. The experimental wavenumber and linewidth for both cases, and their differences $\Delta\omega_{exp}$ and $\Delta\Gamma_{exp}$ are also obtained and shown in Fig. 3(c). The wavenumber and linewidth differences due to the heating ($\Delta\Gamma_{\Delta T}$ and $\Delta\omega_{\Delta T}$), and the focusing effects ($\Delta\Gamma_{focus}$ and $\Delta\omega_{focus}$) are evaluated following the same process for

#184110 - $15.00 USD Received 24 Jan 2013; revised 9 Apr 2013; accepted 2 Jun 2013; published 7 Jun 2013

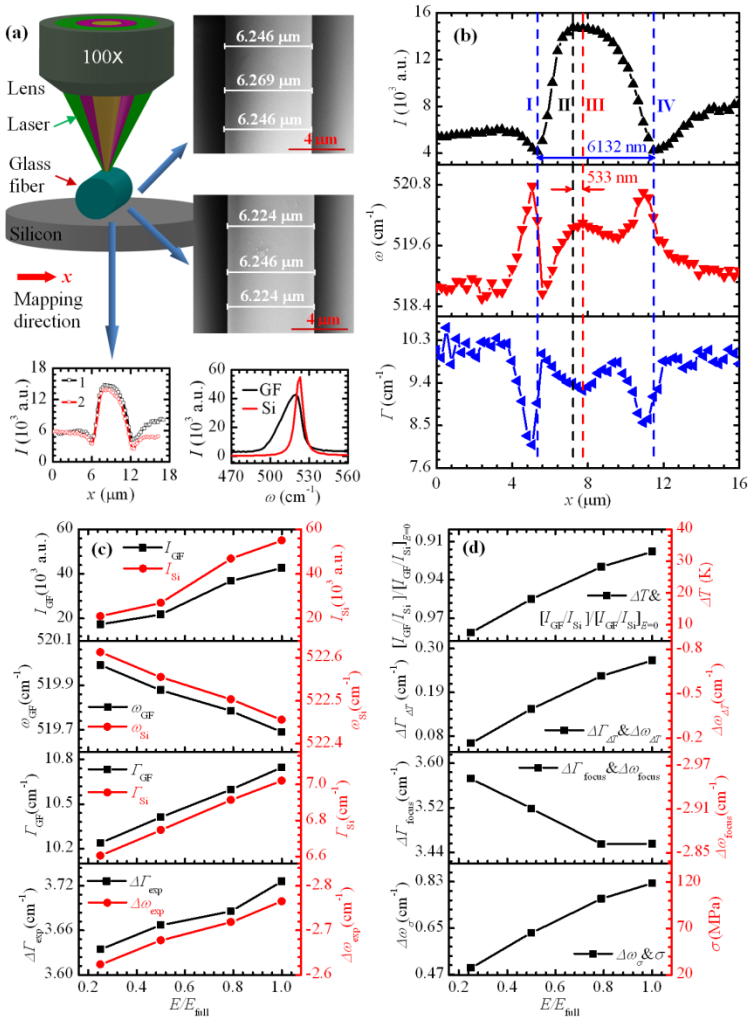

Fig. 3. Raman mapping and thermal probing inside silicon under single-fiber-focused laser irradiation. (a) SEM images of microfiber and Raman spectra and Raman intensity variation in the imaging direction. (b) The x direction variation of Raman intensity I, wavenumber ω, and linewidth Γ for silicon under microfiber with laser irradiation. (c) How Raman data of silicon under glass fiber and that of pure silicon vary with energy percentage. (d) Temperature rise and thermal stress in silicon under different laser energies.

the single silica particle. When the laser energy changes from 25% to 100%, $[I_{GF}/I_{Si}]/[I_{GF}/I_{Si}]_{E=0}$ in Fig. 3(d) reduces from 0.98 to 0.92, ΔT increases from 7.6 to 33.0 K, and $\Delta\omega_\sigma$ increases from 0.5 to 0.8 cm^{-1}. The stress σ which is directly computed from $\Delta\omega_\sigma$ increases from 137 to 230 MPa while E increases from 25% to 100%. Through extrapolation, the calculated stress is 110 MPa at $E=0$. However, it should be zero when the laser is off. There might be some reason that causes the calculated non-zero stress at zero laser energy. To adjust the calculated stresses to meet the reality, all the values are subtracted by 110 MPa. In this case, σ will be zero at $E=0$. The real compressive stress is obtained and shown in the last panel of Fig. 3(d). σ varies from 27 to 120 MPa as E goes up from 25% to 100%. The uncertainty of temperature rise in this case is ± 1.9 K, according to the experimental error of intensity ratio at zero energy (0.00462). The uncertainties of $\Delta\omega_{exp}$ and

#184110 - $15.00 USD Received 24 Jan 2013; revised 9 Apr 2013; accepted 2 Jun 2013; published 7 Jun 2013

$\Delta\omega_{\text{exp}}$ are ± 0.04 cm^{-1} and ± 0.02 cm^{-1}, respectively. The combined standard uncertainty of $\Delta\omega_{\sigma}$ is determined as ± 0.045 cm^{-1}, and the uncertainty of thermal stress is ± 13 MPa.

The thermal stress for the silicon under the glass fiber is higher than that under the silica particle at the same temperature-rise situation. The experimental wavenumber and linewidth in the fiber case vary more linearly with the laser energy than those in the particle case. These phenomena are owing to the diameter difference and focusing effect. When the size of the focusing element is larger, the laser is less focused on the substrate. While changing the laser energy filter in the experiment, there is a little change in the optical alignment, as well as the laser focusing condition. The diameter of glass fiber (6.24 μm) is five time that of silica particle (1.21 μm). So the focusing effect in the glass fiber is smaller, and it is less sensitive to the alignment change and out-of-focus effect. For the fiber case, $\Delta\omega_{\text{exp}}$ and $\Delta\Gamma_{\text{exp}}$ vary more linearly with the laser energy and the changing trends of $\Delta\omega_{\text{focus}}$ and $\Delta\Gamma_{\text{focus}}$ are better than the particle case.

3.3 Physical interpretation of near-field focusing and heating

To understand the mechanism of temperature and stress rise in the silicon substrate under near-field focusing, simulation is performed to obtain the optical, thermal, and stress information. The simulation process and results for the microparticle induced laser heating with the highest energy intensity are outlined below. A uniform laser beam is focused in a substrate by a microparticle. As the silica particle is transparent to green light, the particle absorbs little laser energy. Strong energy absorption occurs in the silicon substrate under the particle within a tiny elliptical zone. The photon's energy is converted into vibrations of the molecules, giving rise of a temperature rise. The resulting thermal expansion of heated silicon is constrained by the nearby cold silicon, which induces a compressive stress in the local region. Optical field simulation for microparticle-induced laser focusing is first conducted using the high frequency structure simulator (HFSS V14). The modeled physical domain consists of a silicon substrate ($\varepsilon = 17.22 + 0.428i$) and a quarter of a 1.21 μm silica particle ($\varepsilon = 2.13 + 0i$) on top of it (in the air). Perfect *H* and Perfect *E* symmetry boundaries are set at symmetrical planes, and radiation boundaries are applied for the other boundary planes. A plane wave ($\lambda = 532$ nm) with an amplitude of 1 V/m is incident normally from the top. Other details of the optical field simulation can be found elsewhere [12]. $I_{\text{si}} = 0.5c\varepsilon_0 nE^2$ is the intensity inside the silicon substrate, where $c = 3\times10^8$ m/s , $\varepsilon_0 = 8.854\times10^{-12}$ F/m , $n = 4.15$, and E (V/m) the magnitude of the electric field. Figure 4(a) shows the optical intensity distribution inside the silicon substrate. In the figure, I_{si}/I_0 indicates the optical intensity enhancement in silicon relative to the incident wave. It is evident that the photon energy is confined to a tiny region near the contacting point between the particle and the substrate with a radius of about 200 nm.

The temperature field distribution inside the silicon substrate is simulated using FLUENT V12. A quarter of cylinder domain with a radius of 5 μm and a height of 10 μm is considered in the simulation. Both vertical cross-sections use symmetric boundary conditions. Because the temperature field is measured at steady state, and the heat dissipation via radiation is small, so the top end surface of silicon is set adiabatic. The peripheral and bottom end surfaces of the domain and the initial temperature of the substrate are set at 300 K. The heat source is imported from the HFSS calculation results. The heat generation rate is $\dot{q} = I\beta$, where *I* is the laser intensity, and β is the absorption coefficient. Other details of the temperature simulation can be found in refs [12, 13]. Figure 4(b) shows the temperature distribution in the silicon substrate. The calculated maximum temperature rise inside the silicon is 51.0 K, agreeing well with the experimental result (58.5 K).

#184110 - $15.00 USD Received 24 Jan 2013; revised 9 Apr 2013; accepted 2 Jun 2013; published 7 Jun 2013

The thermal stress distribution inside the silicon substrate is simulated using ANSYS V14. The model as well as the temperature distribution is imported from the FLUENT calculation. The peripheral and foot end surfaces of the model are fixed. The top boundary is not constrained. Both vertical cross-sections are symmetric. The properties of silicon employed in both temperature and stress modeling are listed in Table 1 [18]. Figure 4(c) shows the thermal stress distribution in silicon. The maximum thermal stress observed in the simulation is 30 MPa, quite different from the experimental value of 160 MPa. There are three main factors that could lead to the difference between experiments and simulation. First, the incident laser employed in the optical field simulation is a uniform plane wave, while in the experiments the laser is focused by a 100× objective lens before it irradiates the sample. Although the laser is still uniformly distributed in space, the direction of propagation has been changed. As a result, the focal size in the experiments could be smaller, and the temperature gradient would be larger. Therefore, the thermal stress can be much higher than the simulation results. Second, when evaluating the experimental stress, the Raman linewidth is assumed entirely stress independent. However, stress may have some effects on the linewidth [19]. Finally, the experimental relationship between wavenumber and linewidth for out-of-focus effect is achieved by using pure silicon around the laser focal spot, which assumes that the out-of-focus effect of silicon within the laser spot is all the same. However, while in the mapping and thermal probing experiments, both silicon signals from in-focus and out-of-focus regions are collected, and only part of the sample is out of focus. In this case, the Raman wavenumber and linewidth in the Gaussian function are actually summations of the two effects. These are different from the wavenumber and linewidth in the Gaussian function used in the out-of-focus calibration, where only out-of-focus status is considered. It leads to some uncertainty in evaluating the out-of-focus effect, which could finally affect the stress calculation.

Table 1. Physical properties of silicon wafer used in modeling

Density	Specific heat	Thermal conductivity	Young's modulus	Thermal expansion coefficient	Poisson's ratio
[kg·m^{-3}]	[J·Kg^{-1}·K^{-1}]	[W·m^{-1}·K^{-1}]	[GPa]	[K^{-1}]	
2329	705	148	117.4	2.62×10^{-6}	0.262

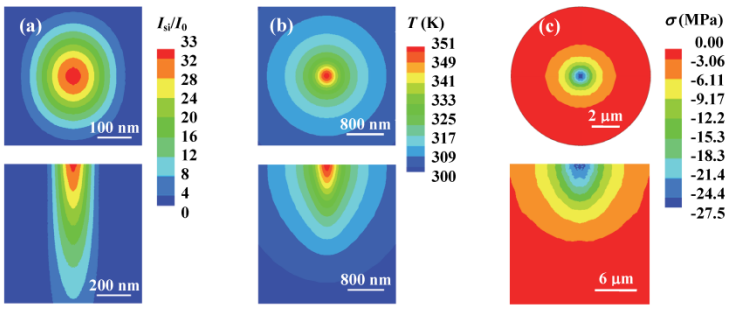

Fig. 4. Optical, thermal, and stress modeling results. (a) Optical intensity distribution inside the silicon substrate. The amplitude indicates the optical intensity enhancement relative to the incident wave. (b) Temperature distribution inside the silicon substrate. The initial temperature in silicon is 300 K. (c) The thermal stress distribution induced by temperature rise inside the silicon substrate. The upper figures show the top of the substrate, and the lower figures show the vertical planes (side-view) in silicon under the particle center.

4. Conclusion

In this work, nanoscale imaging of near-field focusing and heating in a silicon substrate beneath a single silica particle and a glass fiber was conducted for the first time using Raman spectroscopy. Imaging based on Raman intensity, wavenumber, and linewidth all reflected conjugated structural (near-field focusing), thermal, and stress effects. Difference in the

#184110 - $15.00 USD Received 24 Jan 2013; revised 9 Apr 2013; accepted 2 Jun 2013; published 7 Jun 2013

imaging based on these three parameters was largely induced by the non-coincidence between the laser beam axis and the signal collecting axis of the Raman spectrometer. The structural, thermal, and stress effects were de-conjugated to obtain the local temperature rise and stress. Under a single 1.21 μm silica particle, the temperature rise in the near-field focusing region reached 58.5 K under a laser fluence of 3.9×10^9 W/m^2, and the local stress is 160 MPa. The temperature rise and thermal stress in silicon under a 6.24 μm glass fiber induced laser heating were 33.0 K and 120 MPa, respectively. Our study under different energy levels revealed that the temperature rise and local stress increased almost linearly with the energy fluence. The optical, thermal, and stress fields in the substrate were simulated to interpret the experimental results with sound agreement.

Acknowledgments

Support of this work by the National Science Foundation (CMMI-0926704, CMMI-1200397, and CBET-0932573) is gratefully acknowledged. X.W. thanks the great support of the "Taishan Scholar" program of Shandong Province, China.

#184110 - $15.00 USD Received 24 Jan 2013; revised 9 Apr 2013; accepted 2 Jun 2013; published 7 Jun 2013